ES Materials and Manufacturing
DOI: https://dx.doi.org/10.30919/esmm5f861

Effect of B-site Disorder on The Electrical Properties of Barium Zirconium Titanate Ceramics Composites

P. K. Bajpai,[1] C. R. K Mohan,[1] K. N. Singh,[2,*] Anamika Dwivedi,[3] Millan Hait[4,*] and Zhanhu Guo[5]

Abstract

$BaZr_xTi_{1-x}O_3$, Barium zirconium titanate (BZT) samples with x = (0.05, 0.10, and 0.15), were produced via solid solution reactions employing controlled heating and cooling. Sintering temperatures optimized density. XRD reveals phase purity. All patterns have perovskite lines. The homo-valent substitution of Ti (ionic radius = 0.745Å) by Zr (ionic radius = 0.86Å) produces an orthorhombic structure with a higher standard deviation as Zr content increases. Orthorhombic-tetragonal composition with x = 0.15. The ferroelectric phase transition temperature T_c for $BaZr_xTi_{1-x}O_3$ lowers with Zr concentration and exhibits a large peak. Composition-dependent dielectric response occurs in $BaZr_xTi_{1-x}O_3$. The broadened peaks demonstrate disordered perovskite's diffuse transitions. Grain size distribution and quadratic gradients diffuse transition temperatures in ferroelectric ceramics. Due to the difference in electrical density between polar [TiO_6] and non-polar [ZrO_6] clusters, samples with both clusters exhibit this behaviour more strongly. The modified Curie law describes complicated ferroelectrics with diffuse phase transition dielectric behaviour. The material becomes increasingly diffuse and disordered as Zr concentration increases, causing Debye's behaviour to deviate. Low-frequency dielectric dispersion occurs in ferroelectrics with significant ionic conductivity. BZT is being considered for use in capacitors and microwave technologies because of its high dielectric constant, low dielectric loss, and extensive tunability.

Keywords: Ferroelectric; Phase transition; Optimization; Debye behaviour.
Received: 03 December 2022; Revised: 31 March 2023; Accepted: 03 April 2023.
Article type: Research article.

1. Introduction

Barium titanate (BT) is a well-known ferroelectric material below the Curie temperature $T_C \approx 130$ °C, above the Curie-temperature Barium titanate turns into a paraelectric material and has a cubic structure.[1,2] Barium zirconate titanate (BZT) has attracted great attention for its potential applications such as capacitors and microwave technology due to its high dielectric constant, low dielectric loss, and large tunability.[3] The BZT system has been established as one of the most important compositions for dielectrics in multilayer ceramic capacitors.[4] This lead-free relaxor material presents a great interest both for applications in the field of environmental protection and for fundamental studies. In a perovskite structure, a wide range of possible substitutions on B or A sites can change the microstructure, dielectric, piezoelectric, and ferroelectric properties of BZT materials.[5–10] To lower the dielectric loss at low frequencies, Zr^{4+} ions were added to BT to replace Ti^{4+} ions and make BZT.[11]

However, the high dielectric loss at high frequencies exhibited by these ceramics limits their use as a microwave dielectric.[12,13] Currently, Barium zirconate titanate $BaZr_xTi_{1-x}O_3$ (BZT) has been chosen as an alternative material to replace current Pb-based systems and $BaTiO_3$ (BT).[14] In BZT, Zr^{4+} ions are chemically more stable than Ti^{4+} ions and have larger ionic radii to expand the perovskite lattice.[15-22] Therefore, the conduction by electron hopping between Ti^{4+} and Ti^{3+}, if any, would be depressed by such a substitution. Furthermore, it was reported that BZT ceramics showed a broad dielectric peak near T_m owing to the inhomogeneous distribution of Zr ions on Ti sites and mechanical stress in the

[1] *Department of Pure & Applied Physics, Guru Ghasidas Vishwavidyalaya, Bilaspur (C.G.), India-495 009.*
[2] *Department of Physics, OP Jindal University, Punjipathara Raigarh ((C.G.), India- 496109.*
[3] *Department of Physics, YBN University Ranchi, Jharkhand, India-834010.*
[4] *Department of Chemistry, Dr C V Raman University Kota Bilaspur (C.G.), India-495113.*
[5] *Integrated Composites Lab, Department of Mechanical and Construction Engineering, Northumbria University, Newcastle Upon Tyne, NE1 8ST, UK.*
**Email:* kn.singh@opju.ac.in (K.N. Singh), haitmilan@gmail.com (M. Hait)

grain.[19] The BZT solid solutions are also of great interest due the composition dependent nature of their dielectric response. The dielectric studies on BZT suggest normal ferroelectric behaviour in the range $0.0 < x < 0.10$, a diffuse phase transition for $0.10 < x < 0.20$ and non-ferroelectric character for $x > 0.20$.[23] These ceramics are also reported to have diffuse phase transition (relaxors like) behavior in $0.26 \leq x \leq 0.4$ compositional range.[24,25] The transition temperatures of $BaTiO_3$ phases move closer with increase in Zr content in $BaZr_xTi_{1-x}O_3$ and merge near the room temperature for $x \geq 0.15$ composition. The T_c can be modified by using isovalent and aliovalent substitutions.[26] Many interesting results were obtained on the dielectric response in BZT; the variation of T_c was determined by a change in the cell volume; the change of order and the diffuseness of the phase transition in BZT could also be attributed to a cell volume effect.[27] There are several reports available on the structure and electrical behaviour of these ceramics synthesized by conventional solid state and chemical routes.[28–32] Most of the studies on ferroelectric materials have been performed for their structural, electrical, and positive temperature coefficient of resistance (PTCR) characteristics only.[33,34] Comprehensive dielectric studies have been reported on the compound in its ferroelectric phase. But not as much is known about paraelectric dielectric behavior, which is more important for applications.[35]

The purpose of the present work is to optimize the densification (by varying the sintering parameter) and study the temperature and the frequency-dependent dielectric responses of the $BaZr_xTi_{1-x}O_3$ (for $x = 0.05$, 0.10, and 0.15). A composition dependence of T_c for maximum densification is obtained. Results are analyzed in terms of the disorder created at the B-site.

2. Experimental

$BaZr_xTi_{1-x}O_3$, (BZT) samples with varying values of $x = (0.05, 0.10$, and $0.15)$, were prepared through solid solution reactions by the standard double sintering ceramic technique using AR-grade $BaCO_3$ (Merck 99.9%), TiO_2 (Merck 99.5%), and ZrO_2 (Merck 99.9%). Stoichiometric amounts of constituent powders were thoroughly wetted and mixed in acetone for 6 hours in an agate mortar. The homogeneously mixed powders were calcined at 12000 °C for 6 hours in a silicon carbide muffle furnace with a controlled heating and cooling profile. X-ray diffraction patterns of calcined powders were measured using CuKa radiation (l = 1.5418) on an x-ray diffractometer (Rigaku, Miniflex). Calcination was repeated twice. CuKa's contribution was subtracted from each XRD. Calcined powder was pressed into disc-shaped pellets at an isostatic pressure of 100 MPa. Polyvinyl alcohol (PVA) was used as a binder. The pellets were sintered using controlled cooling and heating rates in a programmable furnace. Sintered samples were electroded with silver paste, heated at 500 °C for 1 hour, and cooled down to room temperature before electrical measurements were performed. The capacitance and phase angle were measured using a HIOKI 3532-50 LCR Hi-Tester in the frequency range of 100 Hz to 1 MHz. Temperatures ranged from 350 °C to 1500 °C. The microstructure and grain size distribution of the sintered pellets were studied by scanning electron microscopy using a JEOL JSM-5800 scanning electron microscope at 20 kV. P-E data was recorded using a P-E loop tracer (Marine India Pvt. Limited).

3. Results and discussion

3.1 Structural and microstructural study

Figure 1 shows room temperature XRD patterns of various $BaZr_xTi_{1-x}O_3$ (BZT) compositions sintered at 1260 °C. Sharp and single diffraction peaks different from those of the ingredients indicate the formation of single-phase materials. All the patterns exhibit lines corresponding to the perovskite structure. It is clear that the homovalent substitution of Ti (ionic radius = 0.745) by Zr (ionic radius = 0.86) results in an orthorhombic structure, with the standard deviation increasing as the Zr content increases. The composition with $x = 0.15$ shows an orthorhombic structure as well as a tetragonal structure. Observed x-ray diffraction peaks were indexed using a standard computer program, 'POWD'.[36] The cell parameters were refined by the least-squares method. The estimated crystal structure and lattice parameters obtained from XRD data are shown in Table 1.

The processing parameters in ceramics affect the microstructure, grain growth, and densification; thus, the observed properties of the materials are process parameter dependent. In order to understand the role of sintering as well as optimize it for maximum possible densification, all prepared compositions were sintered at different temperatures in the range of 1220–1300 ºC. Samples sintered at different temperatures were subjected to XRD analysis, and the data were used for calculating the unit cell parameters and the theoretical density. In Table 2, the comparison of the experimental density with the theoretical density of different

Table 1. Lattice parameters and particle size of the samples of different BZT compositions (x= 0.05, 0.1, 0.15).

Structural parameters of BZT Compositions									
Composition	Ba $Zr_{0.05}Ti_{0.95}$ O_3			$BaZr_{0.1}Ti_{0.9}$ O_3			$BaZr_{0.15}Ti_{0.85}$ O_3		
Crystal Structure	Orthorhombic			Orthorhombic			Orthorhombic		
	a(Å)	b(Å)	c(Å)	a(Å)	b(Å)	c(Å)	a(Å)	b(Å)	c(Å)
Unit cell parameters	2.8331	4.0122	3.9552	2.8242	3.9871	3.9317	2.8300	3.9868	3.9288
	±0.00045 Å			±0.00078 Å			±0.00028 Å		
Tolerance Factor	0.91			0.90			0.90		

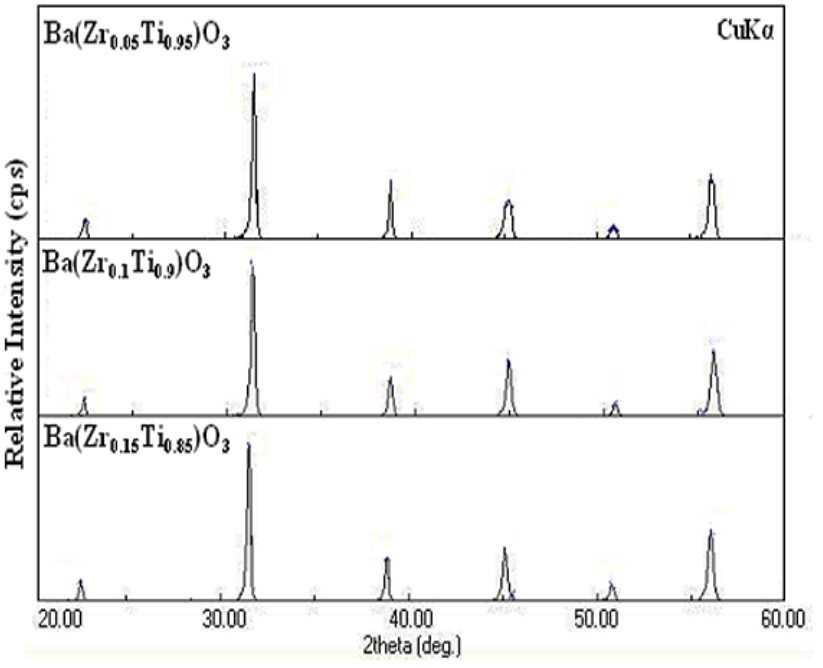

Fig. 1 XRD patterns of Ba $Zr_{0.05}Ti_{0.95}$ O_3 , $BaZr_{0.1}Ti_{0.9}$ O_3 & $BaZr_{0.15}Ti_{0.85}$ O_3 powders Sintered at 1260 ºC for 12 hrs.

Table 2. Comparison of experimental density with theoretical density of different composition at different sintering temperature.

Composition	Sintering temperature (ºC)	Experiment Density (gm/cm^3)	Theoretical density (gm/cm_3)	Relative Density (%)
BZT x= 0.05	1220	5.1862	6.03321	85.96
	1240	4.332	5.975	72.50
	1260	5.3147	5.9833	88.83
	1280	5.0601	6.0509	83.63
	1300	4.2298	5.9542	71.03
BZT x= 0.1	1220	5.4262	6.2007	87.50
	1240	5.407	6.069	89.09
	1260	5.5443	6.056	91.55
	1280	5.4834	6.0691	90.34
	1300	5.1418	6.0393	85.13
BZT x= 0.15	1220	3.2944	6.181	53.29
	1240	5.3689	6.063	88.55
	1260	5.433	6.083	89.31
	1280	5.3494	6.115	87.48
	1300	5.575	6.2027	88.6

compositions at different sintering temperatures is shown. The density increases by increasing the sintering temperature from 1200 ºC up to 1260 ºC. With a further increase in sintering temperature, the experimental density starts to decrease. Thus, at 1260 ºC, the sintering is optimized, and we get maximum density. B-site substitution of Zr^{4+} increases the lattice parameter with increasing Zr content, which may be attributed to the larger ionic radii of Zr^{4+} (ionic radius = 0.86 Å) in comparison to Ti^{4+} (ionic radius = 0.745 Å). The maximum percentage of experimental density achieved was 90% of theoretical density. The SEM micrographs for the studied BZT compositions are shown in Fig. 2. Well-developed large and small grains are clearly visible in the micrographs, with some strain developing on the grains in compositions with x = 0.05 and 0.15. For x = 0.10, the observed grains are almost the same size, are homogeneously distributed, and are spherical, with an average grain size of 2-3 mm at room temperature. For the remaining two compositions (x = 0.05 and 0.15), the average grain sizes are relatively larger (3 to 7 mm). In SEM graphs, no secondary phase was visible.

3.2 Dielectric studies

The dielectric constant and corresponding loss of $BaZr_xTi_{1-x}O_3$ (x = 0.05, 0.1, and 0.15), as a function of temperature at 1 kHz frequency, are shown in Figs. 3 and 4, respectively. In the high temperature phase, the Curie-Weiss law is followed, which is

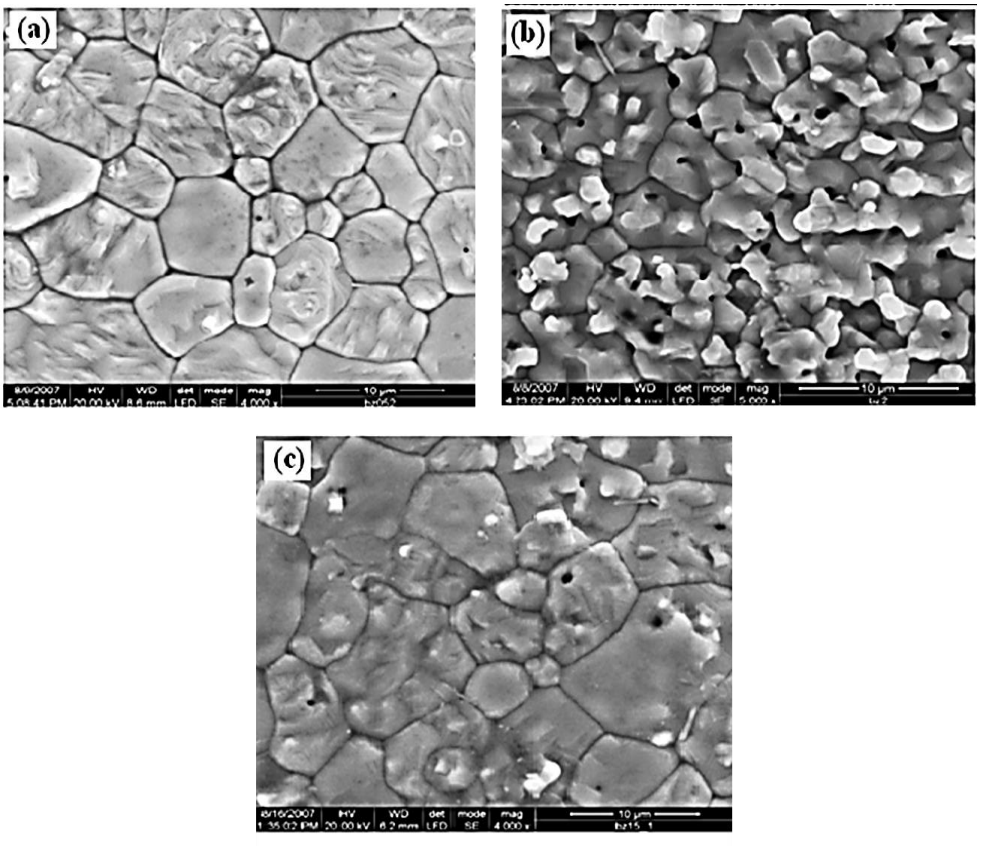

Fig. 2 SEM micrographs of (a) $Ba(Zr_{0.05}Ti_{0.95})O_3$ (b) $Ba(Zr_{0.10}Ti_{0.90})O_3$ and (c) $Ba(Zr_{0.15}Ti_{0.85})O_3$.

compared with the (paraelectric to ferroelectric) phase transition temperature for $BaTiO_3$ (T_c = 393 to 408K). The ferroelectric phase transition temperature T_c for $BaZr_xTi_{1-x}O_3$ shifts towards a lower temperature with increasing Zr concentration and is accompanied by a broad peak. Table 3 shows the variation of the dielectric response as a function of composition for $BaZr_xTi_{1-x}O_3$ (x = 0.05, 0.1, and 0.15). The broadened peaks indicate that the transitions are of the diffuse type, an important characteristic of disordered perovskite. The diffuse transition nature, especially in the case of ferroelectric ceramics, is usually attributed to the grain size distribution and/or a quadratic gradient, leading to a transition temperature distribution. This phenomenon is more pronounced in samples containing both $[TiO_6]$ and $[ZrO_6]$ clusters in their compositions, probably as a consequence of the difference in electronic density between the polar $[TiO_6]$ and non-polar $[ZrO_6]$ clusters. Hence, the additional spatial fluctuations caused by the $[TiO_6]$ and $[ZrO_6]$ clusters in the structure lead to the coexistence of regions with different Curie temperatures, which are dependent on the Ti and Zr concentrations in the solid solution.[37] The Curie constant for each composition is calculated in the paraelectric phase by plotting $1/\varepsilon'$ vs. T as shown in Figs. 5(a-c). The values of the dielectric constant and Curie temperature are given in Table 2. These values agree well with the reported results, with a minor difference as different sintering temperatures could influence the phase transition temperature. There is a linear decrease in T_c with increasing Zr content in BZT compositions, is shown in Fig. 6. The linear fit as shown in Fig. 6 gives T_c= -246 + 360x, which on extrapolation gives T_c = 114 °C for $BaTiO_3$. The values are close to those reported in the literature (T_c =128 °C).[38]

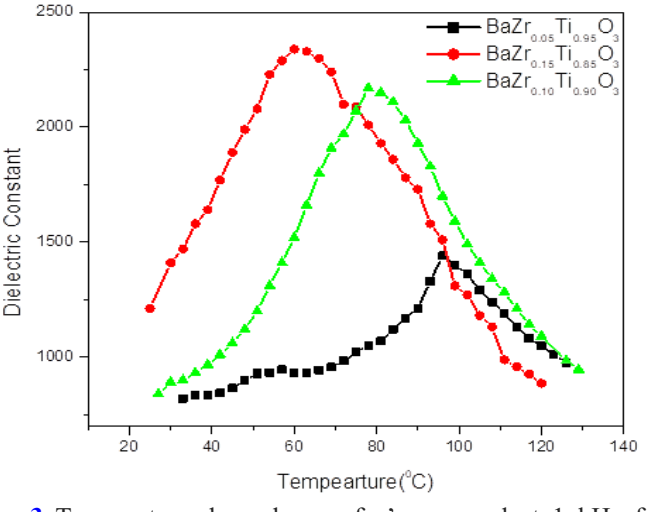

Fig. 3 Temperature dependence of ε' measured at 1 kHz for $BaZr_xTi_{1-x}O_3$ (x= 0.05, 0.1, 0.15) sintered at 1280 °C.

Table 3. Variation of Dielectric response as a function of composition in for $BaZr_xTi_{1-x}O_3$ (BZT) (x= 0.05, 0.1, 0.15).

Sample BZT	Dielectric Peak at	ε'	Loss tangent (tan δ)	Curie constant
X=0.05	96	1440	0.0282	8.53×10^4
X=0.10	78	2170	0.0328	7.07×10^4
X=0.15	60	2340	0.0270	5.29×10^4

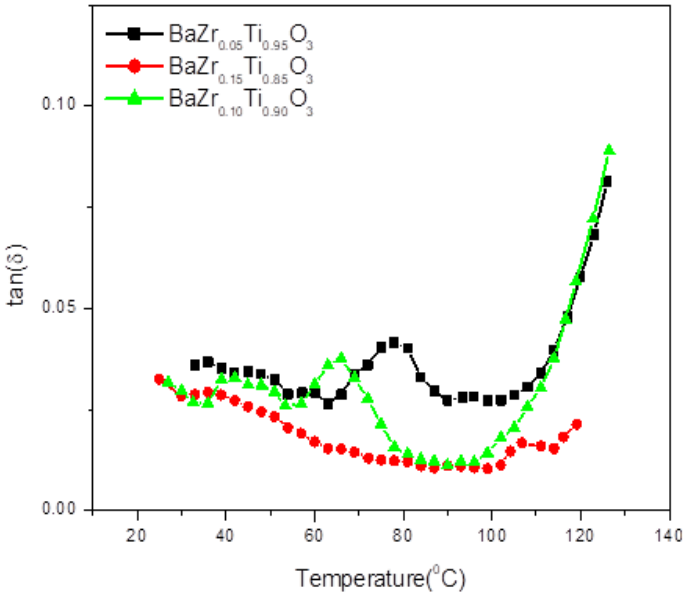

Fig. 4 Variation of tan(δ) (sintered at 1280 ºC) as a function of temperature at 1 kHz for $BaZr_xTi_{1-x}O_3$ (x= 0.05, 0.1, and 0.15).

The tangent losses (Fig. 4) also show peaks in the vicinity of the transition temperature. The loss tangent increases with increasing zirconium content. It also increases at higher temperatures for compositions with a higher Zr content. This indicates that the Zr^{4+} is disordered and relatively more mobile. As shown in Fig. 5(d), all compositions deviate from the Curie-Weiss law, particularly (x = 0.01 and 0.15). This deviation is typical of the behaviour of ferroelectric materials with diffuse phase transitions. A modified Curie law is used to understand the dielectric behaviour of complex ferroelectrics with a diffuse phase transition, described as in Equation 1.[39]

$$\frac{1}{\varepsilon'} - \frac{1}{\varepsilon'_m} = \frac{(T-T_m)^\gamma}{C'} \quad (1)$$

where γ and C' are measured to be constants, and the value of γ lies between 1 and 2. The parameter gives information on the phase transition character, γ = 1 represents classical ferroelectric phase transition where normal Curie-Weiss law is followed, and γ = 2 gives the quadratic dependence that describes complete diffuse phase transition. Fig. 7 shows the plot of log (1/ε – 1/ ε_m) as a function of log (T-T_m) at 1 kHz. A linear relationship is obvious from the plot. The values of γ estimated from the slope of the graphs are 1.25, 1.81, and 1.94 for x = 0.05, 0.1, and 0.15, respectively, indicating that the diffuse phase transition characteristics increase with Zr content. The observed broadness or diffuseness occurs mainly because of the compositional fluctuations and/or structural disorder in the lattice. This may be correlated with the prevailing disorder at B-site due to the two cations (Zr^{4+} and Ti^{4+}) competing at this site.

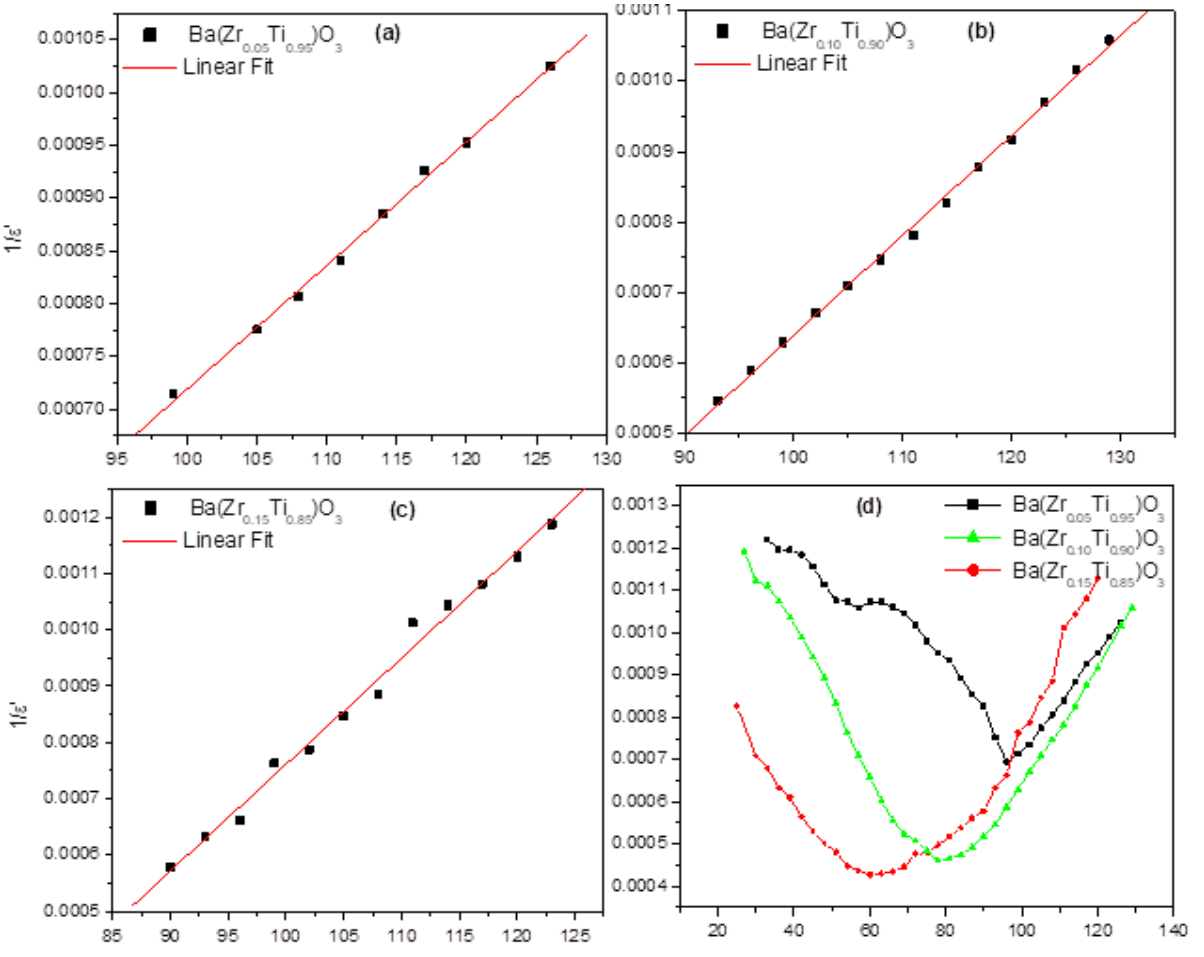

Fig. 5 (a-c) Inverse dielectric constant as a function of temperature in the paraelectric phase for various BZT compositions; (d) the PE-FE phase transition in samples at 1 kHz.

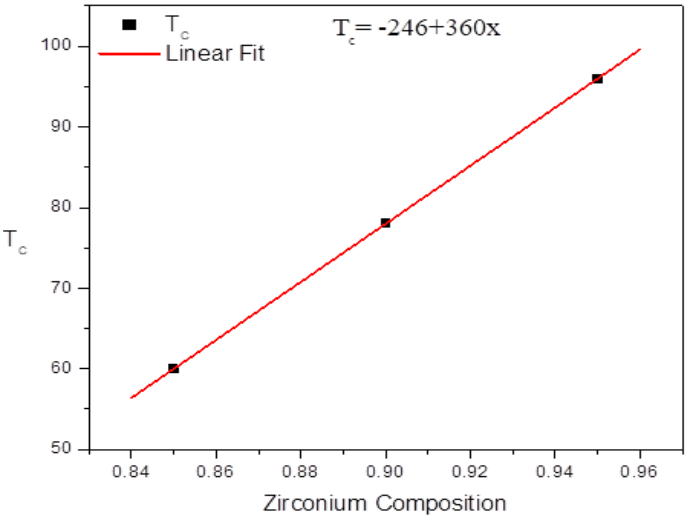

Fig. 6 Variation of transition temperature (T_c) on compositional variation in BZT solid solutions.

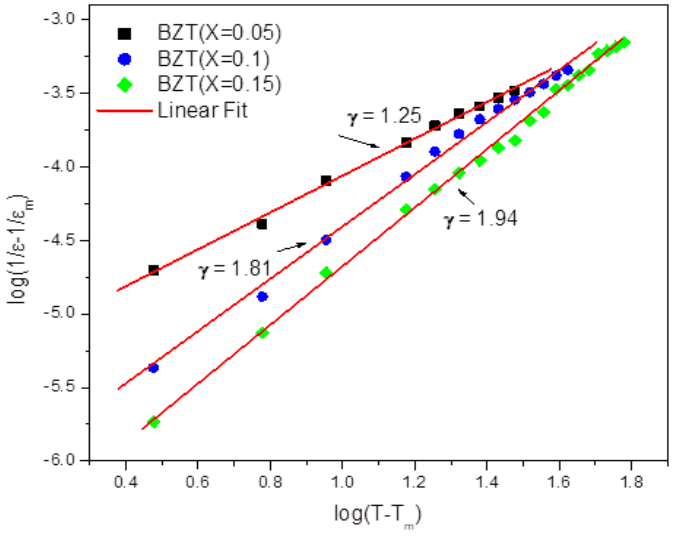

Fig. 7 log $(1/\varepsilon - 1/\varepsilon_m)$ as function of log$(T-T_m)$ for PBN at 1kHz.

The frequency dependence of the dielectric constant and corresponding loss are shown in Figs. 8(a, c, e) and 8(b, d, f), respectively, for BZT (x = 0.05, 0.1, and 0.15) compositions. A general feature of the dielectric response is that dielectric constant values decrease with increasing frequency of excitation and the high frequency dielectric behaviour becomes temperature independent. Dielectric loss shows a peak that varies with temperature. The value of (ε') at lower frequencies, in general, increases with decreasing frequency and increasing temperature. This may be attributed to free charge buildup at the interface between the sample and the electrode (space charge polarization).

For a given temperature, the magnitude of (ε') decreases with increasing frequencies, which is a typical characteristic of disordered materials.[40,41] The Debye formula for complex permittivity related to a free dipole oscillating in an alternating field[42] is explained by the following Equations 2-4.

$$\varepsilon^* = \varepsilon' - j\varepsilon'' = \varepsilon_\infty + \frac{(\varepsilon_s - \varepsilon_\infty)}{1+j\omega\tau} \quad (2)$$

The real part of ε^* is given by:

$$\varepsilon' = \varepsilon_\infty + \frac{(\varepsilon_s - \varepsilon_\infty)}{1+j\omega^2\tau^2} \quad (3)$$

and the imaginary part of ε^* is:

$$\varepsilon'' = \varepsilon_\infty + \frac{(\varepsilon_s - \varepsilon_\infty)\omega\tau}{1+j\omega^2\tau^2} \quad (4)$$

where ε_s and ε_∞ are the low and high frequency values of (ε') (ω), $\omega=2\pi\nu$, ν being the measuring frequency, and τ being the relaxation time. Theoretical fitting of dielectric data (dielectric constant and dielectric loss) is shown in Figs. 9(a, c, e) and 9(b, d, f), respectively, for BZT (x = 0.05, 0.1, and 0.15) compositions. From Fig. 8, it is clear that the experimental behaviour follows the Debye equation. However, the contribution of the dielectric constant is overestimated by the Debye equation, especially at lower frequencies, and the experimentally observed losses are more diffuse than those expected from the single relaxation process of Debye. Deviation from the Debye behaviour increases with an increase in Zr concentration, which is a clear indication of the system becoming more diffuse and disordered in the material. Such dispersion in both components of the complex dielectric constant is commonly observed in ferroelectrics with appreciable ionic conductivity and is referred to as low frequency dielectric dispersion (LFDD).[43,44]

3.3 Ferroelectric properties

The ferroelectric properties of various compositions of BZTs were studied using P–E hysteresis loop data. The typical hysteresis loops below transition temperature (T_c) for all compositions are shown in Fig. 10. For all compositions, a symmetrical hysteresis loop could be observed. All loop measurements are for as-prepared samples without any poling; therefore, the values of spontaneous polarization are less than the reported ones. The ferroelectric loop data is shown in Table 4. However, saturated polarization, the coercive field, and remnant polarization decrease with an increase in Zr concentration.

Table 4. P-E hysteresis loops parameters for various compositions of $BaZr_xTi_{1-x}O_3$ (x=0.05, 0.1, 0.15) below T_c.

Composition	Coercivity (kV/cm)	Remnant Polarization ($\mu C/cm^2$)	E_{Max} field (kV/cm)	Saturated polarization P_s ($\mu C/cm^2$)
$BaZr_{0.05}Ti_{0.95}O_3$				
RT	0.718	3.305	5.041	3.966
50 °C	0.926	3.305	5.618	3.968
$BaZr_{0.10}Ti_{0.90}O_3$				
RT	0.209	0.213	3.705	3.127
50 °C	0.395	0.372	5.601	3.972
$BaZr_{0.15}Ti_{0.85}O_3$				
RT	3.703	1.981	7.151	3.221
50 °C	2.304	1.278	8.041	3.396

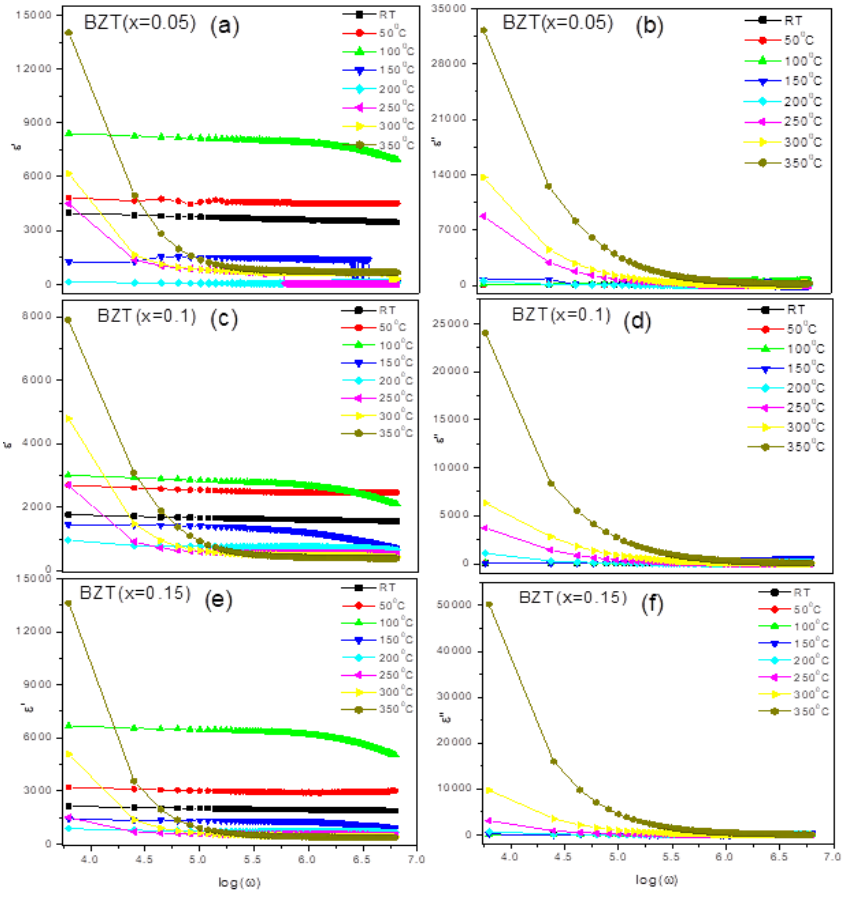

Fig. 8 Frequency dependence of real part ε′ and imaginary part ε″ of dielectric constant at different temperatures for $BaZr_xTi_{1-x}O_3$ (x=0.05, 0.1 and 0.15).

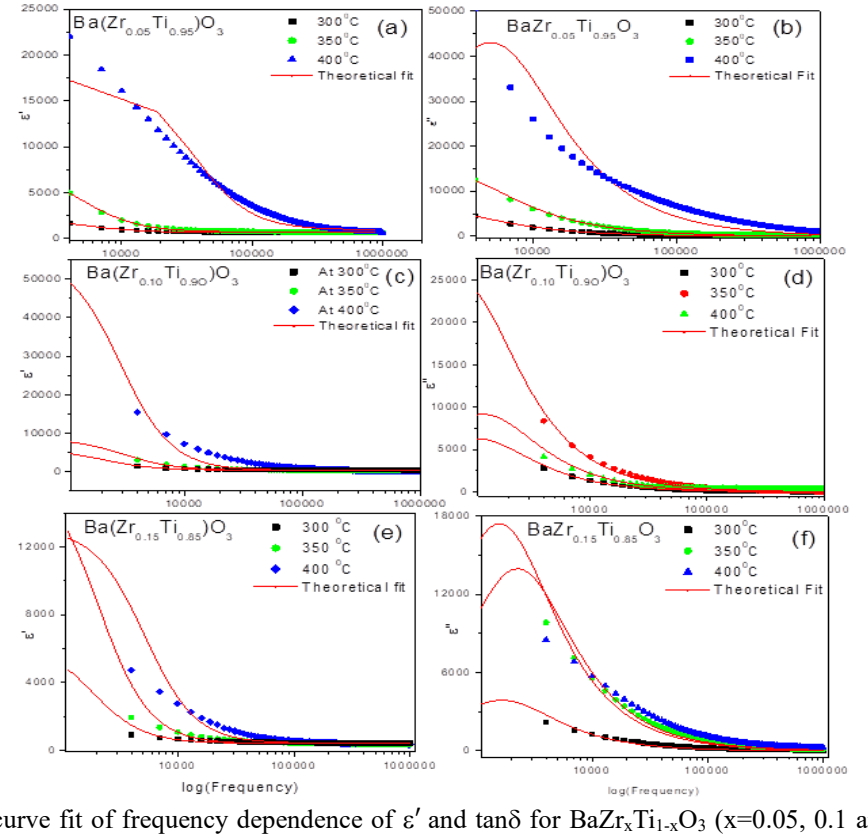

Fig. 9 (a-f) Theoretical curve fit of frequency dependence of ε′ and tanδ for $BaZr_xTi_{1-x}O_3$ (x=0.05, 0.1 and 0.15) using Debye formalism (Equation 3 and 4 in the text). Solid curves are theoretical fits.

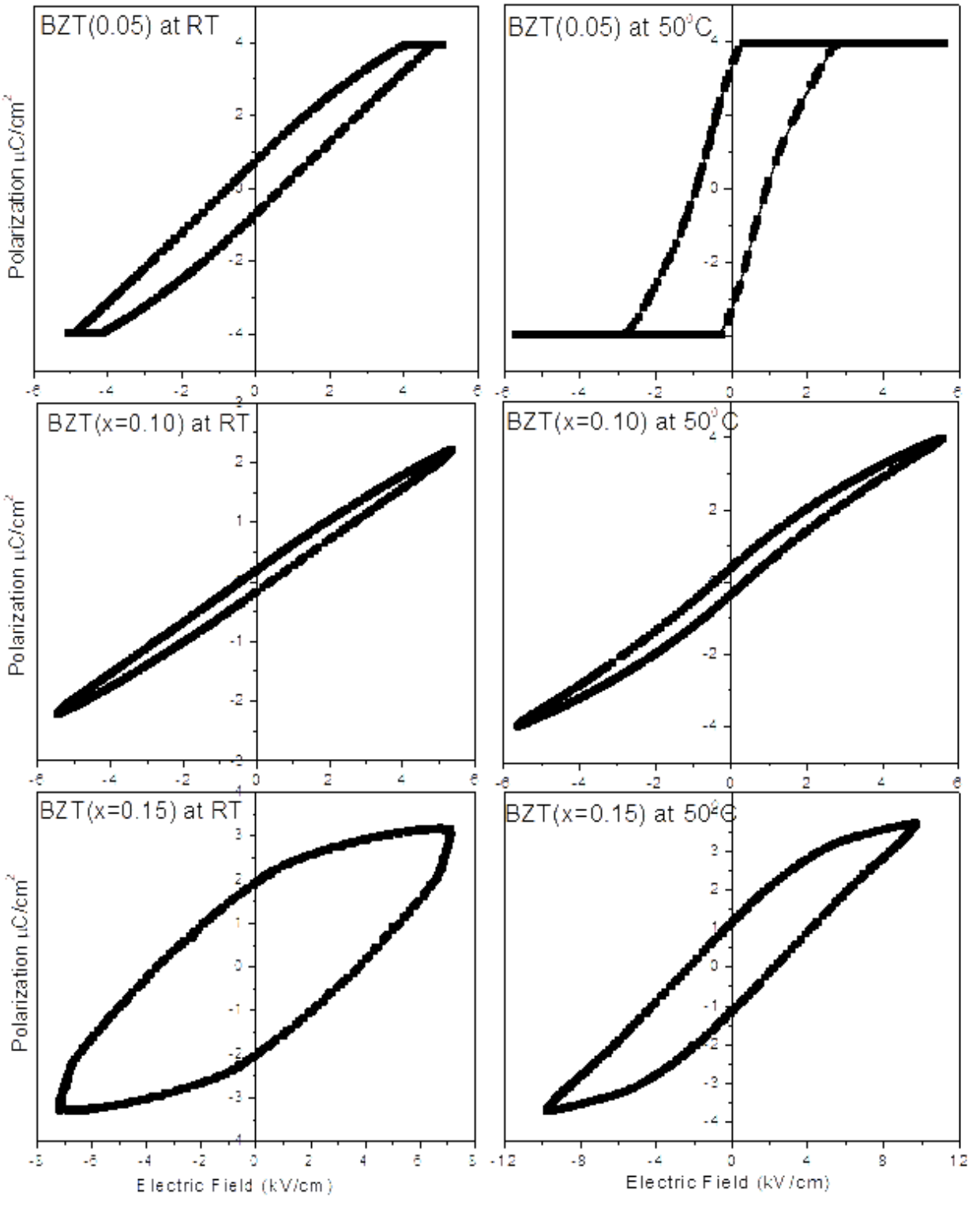

Fig. 10 P-E hysteresis loops observed at various composition of Ba (Zr_xTi_{1-x}) O_3 (x=0.05, 0.1, 0.15) below transition temperature (T_c).

4. Conclusions

$BaZr_xTi_{1-x}O_3$, (BZT) samples with varying values of x = (0.05, 0.10, and 0.15), were prepared through solid solution reactions by the standard double sintering ceramic technique using controlled heating and cooling. The density increases by increasing the sintering temperature from 1200 °C up to 1260 °C. With a further increase in sintering temperature, the experimental density starts to decrease. Thus, at 1260 °C, the sintering is optimized, and we get maximum density. B-site substitution of Zr^{4+} increases the lattice parameter with increasing Zr content, which may be attributed to the larger ionic radii of Zr^{4+} (ionic radius = 0.86 Å) in comparison to Ti^{4+} (ionic radius = 0.745 Å). The maximum percentage of experimental density achieved was 90% of theoretical density.

Well-developed large and small grains are clearly visible in the micrographs, with some strain developing on the grains in compositions with x = 0.05 and 0.15. For x = 0.10, the observed grains are almost the same size, are homogeneously distributed, and are spherical, with an average grain size of 2-3 mm at room temperature. The Debye formula gives complex permittivity related to a free dipole oscillating in an alternating field. Deviation from the Debye behaviour increases with an increase in Zr concentration, which is a clear indication of the system becoming more diffuse and disordered in the material. The ferroelectric properties of various compositions of BZTs were studied using P–E hysteresis loop data.

Conflict of Interest

There is no conflict of interest.

Supporting Information

Not applicable.

References

[1] W. Cai, C. Fu, Z. Lin, X. Deng, Vanadium doping effects on microstructure and dielectric properties of Barium titanate ceramics, *Ceramics International*, 2011, **37**, 3643-3650, doi: 10.1016/j.ceramint.2011.06.024.

[2] K. Niesz, T. Ould-Ely, H. Tsukamoto, D. E. Morse, Engineering grain size and electrical properties of donor-doped Barium titanate ceramics, *Ceramics International*, 2011, **37**, 303-311, doi: 10.1016/j.ceramint.2010.08.040.

[3] T. M. Doan, L. Lu, M. O. Lai, Thickness dependence of structure, tunable and pyroelectric properties of laser-ablated Ba(Zr0.25Ti0.75)O3 thin films, *Journal of Physics D: Applied Physics*, 2010, **43**, 035402, doi: 10.1088/0022-3727/43/3/035402.

[4] D. F. K. Hennings, B. Schreinemacher, H. Schreinemacher, High-permittivity dielectric ceramics with high endurance, *Journal of the European Ceramic Society*, 1994, **13**, 81-88, doi: 10.1016/0955-2219(94)90062-0.

[5] X. Diez-Betriu, J. E. Garcia, C. Ostos, A. U. Boya, D. A. Ochoa, L. Mestres, R. Perez, Phase transition characteristics and dielectric properties of rare-earth (La, Pr, Nd, Gd) doped Ba(Zr0.09Ti0.91)O3 ceramics, *Materials Chemistry and Physics*, 2011, **125**, 493-499, doi: 10.1016/j.matchemphys.2010.10.027.

[6] S. Bhaskar Reddy, K. Prasad Rao, M. S. Ramachandra Rao, Influence of A-site Gd doping on the microstructure and dielectric properties of $Ba(Zr_{0.1}Ti_{0.9})O_3$ ceramics, *Journal of Alloys and Compounds*, 2011, **509**, 1266-1270, doi: 10.1016/j.jallcom.2010.09.211.

[7] W. Cai, J. Gao, C. Fu, L. Tang, Dielectric properties, microstructure and diffuse transition of Ni-doped $Ba(Zr_{0.2}Ti_{0.8})O_3$ ceramics, *Journal of Alloys and Compounds*, 2009, **487**, 668-674, doi: 10.1016/j.jallcom.2009.08.034.

[8] T. Badapanda, S. K. Rout, L. S. Cavalcante, J. C. Sczancoski, S. Panigrahi, T. P. Sinha, E. Longo, Structural and dielectric relaxor properties of yttrium-doped $Ba(Zr_{0.25}Ti_{0.75})O_3$ ceramics, *Materials Chemistry and Physics*, 2010, **121**, 147-153, doi: 10.1016/j.matchemphys.2010.01.008.

[9] T.-A. Jain, K.-Z. Fung, S. Hsiao, J. Chan, Effects of BaO-SiO2 glass particle size on the microstructures and dielectric properties of Mn-doped $Ba(Ti, Zr)O_3$ ceramics, *Journal of the European Ceramic Society*, 2010, **30**, 1469-1476, doi: 10.1016/j.jeurceramsoc.2009.11.006.

[10] P. Jarupoom, K. Pengpat, G. Rujijanagul, Enhanced piezoelectric properties and lowered sintering temperature of $Ba(Zr_{0.07}Ti_{0.93})O3$ by B_2O_3 addition, *Current Applied Physics*, 2010, **10**, 557-560, doi: 10.1016/j.cap.2009.07.020.

[11] J. Z. Xin, C.W. Leung, H. L. W. Chan, Composition dependence of structural and optical properties of Ba(Zrx, Ti1-x)O3 thin films grown on MgO substrates by pulsed laser deposition, *Thin Solid Films*, 2011, **519**, 6313-6318, doi: 10.1016/j.tsf.2011.04.007.

[12] A. K. Tagantsev, V. O. Sherman, K. F. Astafiev, J. Venkatesh, N. Setter, Ferroelectric materials for microwave tunable applications, *Journal of Electroceramics*, 2003, **11**, 5-66, doi: 10.1023/B: JECR.0000015661.81386.e6.

[13] F. Zimmermann, M. Voigts, W. Menesklou, E. Ivers-Tiffée, $Ba_{0.6}Sr_{0.4}TiO_3$ and $BaZr_{0.3}Ti_{0.7}O_3$ thick films as tunable microwave dielectrics, *Journal of the European Ceramic Society*, 2004, **24**, 1729-1733, doi: 10.1016/s0955-2219(03)00481-3.

[14] M. Voigts, W. Menesklou, E. Ivers-Tiffee, Dielectric properties and tunability of BST and BZT thick films for microwave applications, *Integrated Ferroelectrics*, 2001, **39**, 383-392, doi: 10.1080/10584580108011962.

[15] Z. Yu, C. Ang, R. Guo, A. S. Bhalla, Dielectric properties and high tunability of $Ba(Ti_{0.7}Zr_{0.3})O_3$ ceramics under dc electric field, *Applied Physics Letters*, 2002, **81**, 1285-1287, doi: 10.1063/1.1498496.

[16] Z. Yu, R. Guo, A. S. Bhalla, Orientation dependence of the ferroelectric and piezoelectric behavior of $Ba(Ti_{1-x}Zr_x)O_3$ single crystals, *Applied Physics Letters*, 2000, **77**, 1535-1537, doi: 10.1063/1.1308276.

[17] J. Ravez, C. Broustera, A. Simon, Lead-free ferroelectric relaxor ceramics in the $BaTiO_3$-$BaZrO_3$-$CaTiO_3$ system, *Journal of Materials Chemistry*, 1999, **9**, 1609-1613, doi: 10.1039/a902335f.

[18] G. X, Tang, Structural, dielectric and optical properties of $Ba(Ti, Zr)O_3$ thin films prepared by chemical solution deposition, *Thin Solid Films*, 2004, **460**, 227-231, doi: 10.1016/j.tsf.2004.01.071.

[19] U. Weber, G. Greuel, U. Boettger, S. Weber, D. Hennings, R. Waser, Dielectric properties of Ba(Zr, Ti)O3-based ferroelectrics for capacitor applications, *Journal of the American Ceramic Society*, 2001, **84**, 759-766, doi: 10.1111/j.1151-2916.2001.tb00738.x.

[20] Ph, Sciau, X-ray diffraction study of $BaTi^{0.65}Zr_{0.35}O_3$ and $Ba_{0.92}Ca_{0.08}Ti_{0.75}Zr_{0.25}O_3$ compositions: influence of electric field, *Solid State Communications*, 1999, **113**, 77-82, doi: 10.1016/S0038-1098(99)00445-7.

[21] X. G. Tang, K. H. Chew, H. L. W. Chan Diffuse phase transition and dielectric tunability of $Ba(Zr_yTi_{1-y})O_3$ relaxor ferroelectric ceramics, *Acta Materialia*, 2004, **52**, 5177-5183, doi: 10.1016/j.actamat.2004.07.028.

[22] Y. Zhi. A Chen, R. Guo, A. S. Bhalla, Ferroelectric-relaxor behavior of $Ba(Ti_{0.7}Zr_{0.3})O_3Ba(Ti_{0.7}Zr_{0.3})O_3$ ceramics, *Journal of Applied Physics*, 2002, **92**, 2655, doi: 10.1063/1.1495069
[23] J. Zhai, X. Yao, L. Zhang, B. Shen, Dielectric nonlinear characteristics of $Ba(Zr_{0.35}Ti_{0.65})O_3$ thin films grown by a Sol-gel process, *Applied Physics Letters*, 2004, **84**, 3136-3138, doi: 10.1063/1.1715152.
[24] Z. Yu, R. Guo, A. S. Bhalla, Dielectric behavior of $Ba(Ti_{1-x}Zr_x)O_3$ single crystals, *Journal of Applied Physics*, 2000, **88**, 410-415, doi: 10.1063/1.373674.
[25] Z. Jing, C. Ang, Z. Yu, P. M. Vilarinho, J. L. Baptista, Dielectric properties of $Ba(Ti_{1-y}Y_y)O_3$ ceramics, *Journal of Applied Physics*, 1998, **84**, 983-986, doi: 10.1063/1.368164.
[26] Z. Jing, Z. Yu, C. Ang, Crystalline structure and dielectric behavior of (Ce, Ba)TiO_3 ceramics, *Journal of Materials Research*, 2002, **17**, 2787-2793, doi: 10.1557/JMR.2002.0405.
[27] R. Roy, Ceramics by the solution-Sol-gel route, *Science*, 1987, **238**, 1664-1669, doi: 10.1126/science.238.4834.1664.
[28] K. W. Kirby, Alkoxide synthesis techniques for $BaTiO_3$, *Materials Research Bulletin*, 1988, **23**, 881-890, doi: 10.1016/0025-5408(88)90082-7.
[29] D. Segal, Chemical synthesis of ceramic materials, *Journal of Materials Chemistry*, 1997, **7**, 1297-1305, doi: 10.1039/a700881c.
[30] B. J. Mulder, Preparation of $BaTiO_3$ and other ceramic powders by coprecipitation of citrates in an alcohol, *American Ceramic Society Bulletin*, 1970, **49**, 990.
[31] M. Stockenhuber, H. Mayer, J. A. Lercher, Preparation of Barium titanates from oxalates, *Journal of the American Ceramic Society*, 1993, **76**, 1185-1190, doi: 10.1111/j.1151-2916.1993.tb03738.x.
[32] T. V. Anuradha, S. Ranganathan, T. Mimani, K. C. Patil, Combustion synthesis of nanostructured Barium titanate, *Scripta Materialia*, 2001, **44**, 2237-2241, doi: 10.1016/s1359-6462(01)00755-2.
[33] R. E. Cohen, Surface effects in ferroelectrics: periodic slab computations for $BaTiO_3$, *Ferroelectrics*, 1997, **194**, 323-342, doi: 10.1080/00150199708016102.
[34] J. Gao, L. Zheng, X. Duo, J. Huang, C. Lin, R. Yan, Total dose radiation effects of $Au/PbZr_{0.52}Ti_{0.48}O_3/YBa_2Cu_3O_{7-\delta}/LaAlO_3$ ferroelectric capacitors, *Radiation Effects and Defects in Solids*, 1998, **145**, 319-327, doi: 10.1080/10420159808223999.
[35] R.-H. Liang, X.-L. Dong, Y. Chen, F. Cao, Y.-L. Wang, Dielectric properties and tunability of $Ba(Zr_xTi_{1-x})O_3$ ceramics under high DC electric field, *Ceramics International*, 2007, **33**, 957-961, doi: 10.1016/j.ceramint.2006.02.009.
[36] E. L. Wu, POWD, an interactive program for powder diffraction data interpretation and indexing, *Journal of Applied Crystallography*, 1989, **22**, 506-510, doi: 10.1107/S0021889889005066.
[37] S. Bhaskar Reddy, K. Prasad Rao, M. S. Ramachandra Rao, Structural and dielectric characterization of Sr substituted Ba(Zr, Ti)O3 based functional materials, *Applied Physics A*, 2007, **89**, 1011-1015, doi: 10.1007/s00339-007-4208-1.
[38] F. Batllo, E. Duverger, J.-C. Jules, J.-C. Niepce, B. Jannot, M. Maglione, Dielectric and E.P.R. studies of Mn-doped Barium titanate, *Ferroelectrics*, 1990, **109**, 113-118, doi: 10.1080/00150199008211399.
[39] G. S. Fulcher, Analysis of recent measurements of the viscosity of glasses, *Journal of the American Ceramic Society*, 1925, **8**, 339-355, doi: 10.1111/j.1151-2916.1925.tb16731.x.
[40] M. Pastor, P. K. Bajpai, R. N. P. Choudhary, Microstructural and electrical study of mixed phase of $Pb(Ba_{1/3}Nb_{2/3})O_3$, *Physica B: Condensed Matter*, 2007, **391**, 1-5, doi: 10.1016/j.physb.2006.02.025.
[41] M. Pastor, P. K. Bajpai, R. N. P. Choudhary, Synthesis and structural characterization of some $Pb(B_1^{3/t}\ Nb_{2/3})O_3$ type materials by two-stage solid-state route, *Bulletin of Materials Science*, 2005, **28**, 199-203, doi: 10.1007/BF02711247.
[42] A. Chelkowski, Dielectric Physics, In "Studies in Physical and Theoretical Chemistry", Vol. 9, Elsevier Scientific Pub. Co. Amsterdam, 1980, 119.
[43] Z. Lu, J. Bonnet, J. Ravez, P. Hagenmuller, Correlation between low frequency dielectric dispersion (LFDD) and impedance relaxation in ferroelectric ceramic $Pb_2KNb_4TaO_{15}$, *Solid State Ionics*, 1992, **57**, 235-244, doi: 10.1016/0167-2738(92)90153-g.
[44] T. A. Nealon, Low-frequency dielectric responses in PMN-type ceramics, *Ferroelectrics*, 1987, **76**, 377-382, doi: 10.1080/00150198708016958.